Low-temperature spin dynamics in the TmFeO_{3} orthoferrite with a non-Kramers ion

S. A. Skorobogatov, S. E. Nikitin, K. A. Shaykhutdinov, A. D. Balaev, K. Yu. Terentjev, G. Ehlers, G. Sala, E. V. Pomjakushina, K. Conder, and A. Podlesnyak

Phys. Rev. B **101**, 014432 — Published 22 January 2020

DOI: 10.1103/PhysRevB.101.014432

Low-temperature spin dynamics in $TmFeO_3$ orthoferrite with non-Kramers ion

S. A. Skorobogatov,[1,2] S. E. Nikitin,[3,4] K. A. Shaykhutdinov,[1] A. D. Balaev,[1] K. Yu. Terentjev,[1] G. Ehlers,[5] G. Sala,[6] E. V. Pomjakushina,[7] K. Conder,[7] and A. Podlesnyak[6,*]

[1] *Kirensky Institute of Physics, Federal Research Center KSC SB RAS, Krasnoyarsk, 660036 Russia*
[2] *Siberian Federal University, Krasnoyarsk, 660041 Russia*
[3] *Max Planck Institute for Chemical Physics of Solids, D-01187 Dresden, Germany*
[4] *Institut für Festkörper- und Materialphysik, Technische Universität Dresden, D-01069 Dresden, Germany*
[5] *Neutron Technologies Division, Oak Ridge National Laboratory, Oak Ridge, TN 37831, USA*
[6] *Neutron Scattering Division, Oak Ridge National Laboratory, Oak Ridge, Tennessee 37831, USA*
[7] *Laboratory for Multiscale Materials Experiments, Paul Scherrer Institut, CH-5232 Villigen PSI, Switzerland*

We investigate the magnetic dynamics of the orthorhombic perovskite $TmFeO_3$ at low temperatures, below the spin reorientation transition at $T_{SR} \approx 80$ K, by means of time-of-flight neutron spectroscopy. We find that the magnetic excitation spectrum combines two emergent collective modes associated with different magnetic sublattices. The Fe subsystem orders below $T_N \sim 632$ K into a canted antiferromagnetic structure and exhibits sharp, high-energy magnon excitations. We describe them using linear spin-wave theory, and reveal a pronounced anisotropy between in- and out-of-plane exchange interactions, which was mainly neglected in previous reports on the spin dynamics in orthoferrites. At lower energies, we find two crystalline electrical field (CEF) excitations of Tm^{3+} ions at energies of ~ 2 and 5 meV. In contrast to the sister compound $YbFeO_3$, where the Yb^{3+} ions form quasi one-dimensional chains along the c axis, the Tm excitations show dispersion along both directions in the $(0KL)$ scattering plane. Analysis of the neutron scattering polarization factor reveals a longitudinal polarization of the 2 meV excitation. To evaluate the effect of the CEF on the Tm^{3+} ions, we perform point-charge model calculations, and their results quantitatively capture the main features of Tm single-ion physics, such as energies, intensities and polarization of the CEF transitions, and the type of magnetic anisotropy.

I. INTRODUCTION

It is well recognized that quantum effects are most pronounced with the smallest possible spin. Here the quantum fluctuations may prevent long-range magnetic ordering even at zero temperature. In recent years, a wide variety of spin-1/2 and spin-1 quantum many-particle models with exotic disordered ground states have been extensively developed [1]. Accordingly, theoretical studies examined key concepts for exotic quantum matter, as for instance, a quantum spin liquid [2], fractional excitations (spinons) and their confinement [3–5], quantum criticality [1, 6], and Bose-Einstein condensation [7–9]. For a long time, the search for a physical realization of novel quantum phases was mainly limited by materials with $3d$ transition metals, mostly Cu^{2+} or Co^{2+}, as a magnetic ion. Remarkable examples include $CaCu_2O_3$ as a realization of the confinement idea [5], fractional spin-1/2 quasiparticles in $CuSO_4 \cdot 5D_2O$ [10], $SrCo_2V_2O_8$ as a paradigm for spinon confinement [11] (see also a recent review in ref. 12 and references therein).

The large anisotropic rare-earth $4f$ moments with strong spin-orbit coupling are normally considered to be 'classical' as temperature $T \to 0$, comparing to the isotropic Heisenberg spin-1/2. However, this is usually in the context of single ion physics, and the crystalline environments may change the electronic properties of the rare-earth ions considerably. Experimental hallmarks of exotic quantum states have been recently reported in number of Yb-based ($4f^{13}$) compounds by the observation of Tomonaga-Luttinger liquid behavior and spinon confinement-deconfinement transitions in $YbAlO_3$ [13]; spinon continuum and spinon confinement in Yb_2Pt_2Pb [14, 15] and in the triangular-lattice systems $YbMgGaO_4$ [16, 17]; the quantum dimer magnet state in $Yb_2Si_2O_7$ [18] and a Higgs transition from a magnetic Coulomb liquid to a ferromagnet in $Yb_2Ti_2O_7$ [19]. In the rare-earth orthoferrite $YbFeO_3$ the Yb magnetic sublattice also exhibits rich quantum spin dynamics [20]. At temperatures below the iron spin-reorientation (SR) transition $T_{SR} = 7.6$ K the Yb spin chains have a well defined field-induced ferromagnetic (FM) ground state, and the spectrum consists of a sharp single-magnon mode, a two-magnon bound state, and a two-magnon continuum, whereas at $T > T_{SR}$ a gapped broad spinon-like continuum dominates the spectrum.

All these experiments exploit the idea that energy levels of the rare-earth ion with an odd number of electrons in the unfilled $4f$ shell (Kramers ions) are split by the crystal field (CF) into doubly degenerate states. The quantum states of the ground Kramers doublet, separated by a large energy gap from the first excited state, can be viewed as an effective spin-1/2 [14]. It was predicted and demonstrated experimentally that the magnetic properties at low temperatures and in low magnetic fields can be described by a pseudospin $S = 1/2$ model [13, 14, 17, 20].

On the other hand, in the case of non-Kramers ions, the

* Corresponding author: podlesnyakaa@ornl.gov

CF splitting may result in singlets, doublets or pseudo-doublets, depending on the symmetry. Accordingly, we can expect rich magnetic field–temperature phase diagrams for compounds with non-Kramers rare-earth ions.

The rare-earth orthoferrites, even though thoroughly studied in past, offer new opportunities for this type of research. In particular, the absence of the long range magnetic order in the rare-earth sublattice down to millikelvin temperatures plays an important role. It was shown recently that the coupling within the rare-earth subsystem in Yb-based orthorhombic perovskites is essentially quasi one-dimensional [13, 20, 21], which results in unusual spin dynamics on the low-energy scale. Experiments to reveal the nature of the rare-earth magnetic state as well as intra- and inter-sublattice correlations have so far been limited and were mainly concerned for single-ion CF considerations.

The aim of this study is to present a quantitative analysis of the magnetic excitations in the orthoferrite $TmFeO_3$, with a non-Kramers rare-earth ion, and to compare the results to the Kramers ion case, $YbFeO_3$ [20] and $YbAlO_3$ [13, 21]. Our target compound is $TmFeO_3$, in which the Tm sublattice does not exhibit long range magnetic order down to $T = 1.6$ K [22]. $TmFeO_3$ crystallizes in an orthorhombic distorted perovskite structure (space group $Pbnm$) [23]. The Fe magnetic sublattice orders antiferromagnetically (AFM) at $T_N \sim 632$ K in a G-type structure (see Fig. 3) [24]. In addition to the AFM structure, the Dzyaloshinskii-Moriya (DM) interaction induces a Fe spin canting giving rise to a weak FM moment. The iron sublattice exhibits the SR transition at 82 K $\lesssim T_{SR} \lesssim$ 93 K when the Fe moments coherently rotate from the a to the c axis [22].

II. EXPERIMENTAL DETAILS

Polycrystalline $TmFeO_3$ was prepared by a solid state reaction following a standard procedure (see, for instance, Ref. [25]). The phase purity of the resulting compound was checked with a conventional x-ray diffractometer. The crystal growth was carried out using an optical floating-zone method (see [20] for details).

Magnetic measurements were carried out using a vibrating-sample magnetometer with a superconducting solenoid in fields up to 7 T and temperatures down to 4.2 K.

The single crystal inelastic neutron-scattering (INS) measurements were performed in wide ranges of reciprocal space and energy transfer to fully map out the excitations of both, Fe and Tm, magnetic sublattices. The INS experiments were performed using two time-of-flight (TOF) spectrometers: the wide angular-range chopper spectrometer (ARCS) [26] and the Cold Neutron Chopper Spectrometer (CNCS) [27, 28], both at the Spallation Neutron Source at ORNL. The data were collected from a single crystal with a mass of around 3.0 g, which was aligned in the $(0KL)$ scattering plane. The incident neutron energy was fixed at $E_i = 100$ and 25 meV (ARCS) and $E_i = 12$ and 3.3 meV (CNCS).

The software packages Dave [29], Horace [30] and MantidPlot [31] were used for data reduction and analysis. Linear spin-wave theory (LSWT), as realized in the SpinW program package [32], was used to calculate the excitation spectra and neutron scattering cross section of the spin Hamiltonian. The crystal electric field (CEF) calculations were performed using the McPhase software package [33].

III. RESULTS AND ANALYSIS

A. High-energy excitations

In this section we discuss the spin dynamics of $TmFeO_3$ associated with the magnon modes of the iron subsystem. To obtain the high-energy magnon spectra we performed INS measurements of $TmFeO_3$ using the ARCS instrument at SNS. Fig. 1 (a) shows an energy-momentum plot along three high-symmetry directions taken with $E_i = 100$ meV. One can see that the spectrum consists of a sharp, well-defined magnon mode, which extends up to ~ 60 meV and can be associated with the spin-wave excitations within the Fe subsystem [20, 25, 34]. However, the low-energy part of the spectrum was rather noisy due to the proximity of the elastic line and strong excitations within the Tm subsystem, and in order to resolve the magnon gap we performed an additional measurement with $E_i = 25$ meV. The cuts close to the Γ-point of the magnetic Brillouin zone along three main axes of reciprocal space are shown in Fig. 1(b-d). One can see that the spectra contain dispersionless bright lines at $E \approx 2$ and 5 meV due to Tm subsystem (which will be discussed in details below in Sec. III B) and the low-energy part of the Fe magnon excitations. It is clear that the Fe magnons have a gap of about 8 meV, its precise determination is difficult because at the Γ-point the magnon mode merges with the Tm CEF excitation.

To quantitatively calculate the underlying exchange interactions we determined the position of the magnon mode at 94 points of reciprocal space [35] and then used this dataset for the fitting to our spin-wave model.

To describe the spin dynamics of the Fe subsystem of $TmFeO_3$ we used the SpinW package [32] and a standard spin Hamiltonian, which included the Heisenberg exchange interactions and an effective anisotropy constant [36]:

$$\mathcal{H} = \sum_{\langle i,j \rangle} J_{ij} \mathbf{S}_i \mathbf{S}_j + K_c \sum_i \mathbf{S}_i. \quad (1)$$

The summation in the first term runs over different sets of neighboring Fe ions as discussed below. The K_c is an effective anisotropy constant, which stabilizes the low-temperature Γ2 ground state. Note, that the K_c is not a simple single-ion anisotropy constant, but also effectively

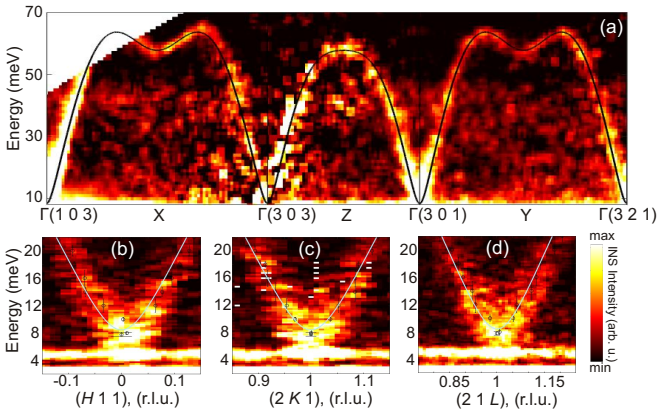

FIG. 1. INS spectra of $TmFeO_3$ measured at $T = 7$ K. (a) Energy-momentum cut through the high-symmetry directions measured with $E_i = 100$ meV. The data were integrated by ± 0.1 Å^{-1} in the orthogonal directions. (b-d) Energy-momentum cuts along H, K and L directions close to the Γ point of the magnetic Brillouin zone show the magnon gap. The spectra were taken with $E_i = 25$ meV and integrated by ~ 0.04 r.l.u. in the orthogonal directions. The solid lines shown in all panels represent the results of the spin-wave calculations as described in a main text.

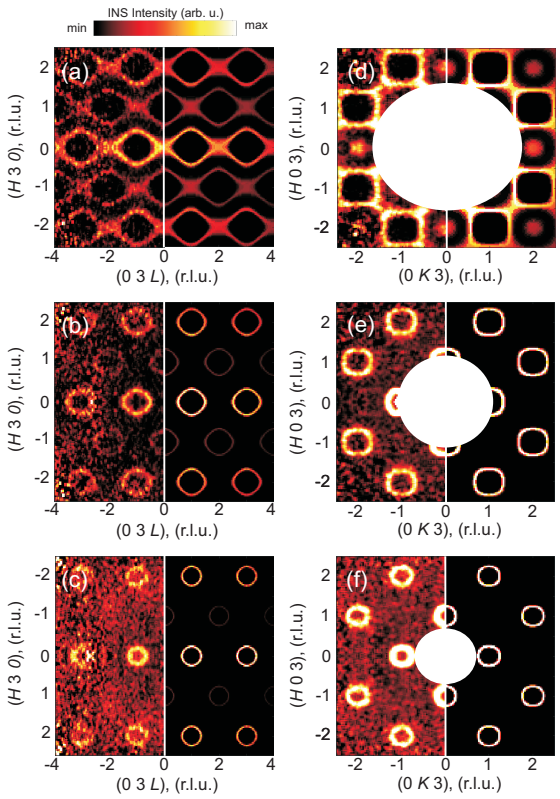

FIG. 2. Constant energy slices of the INS intensity within $(H3L)$ (a-c) and $(HK3)$ (d-f) planes taken at $T = 7$ K. The left and right sides of each panel show the measured and calculated intensities, respectively. The data were integrated within the energy windows of $E = [55.5, 58.5]$ meV (a,d); $E = [45.5, 48.5]$ meV (b,e); $E = [35.5, 38.5]$ meV (c,f).

takes into account rare-earth - Fe interactions, for details see [20].

In the ideal cubic perovskite structure, the Fe ions would have 6 nearest neighbors at a distance equal to the lattice parameter a_0 (here a_0 is a lattice parameter of a perfect cubic structure), and 12 next-nearest neighbors at a distance of $\sqrt{2}a_0$, and one can naturally associate exchange interactions J_1 and J_2 to these bonds. $TmFeO_3$ crystallizes into a distorted orthorhombic structure, which makes the bonds along the different directions nonequivalent. In the general case, when one takes into account $6 + 12$ neighbors, one has to consider 6 nonequivalent exchange interactions as shown in Fig. 3. Previously, the anisotropy of the exchange interactions was not considered, when studying the spin dynamics of $R FeO_3$, assuming:

$$\begin{aligned} J_1 &\equiv J_{1a} = J_{1b} = J_{1c} \,, \\ J_2 &\equiv J_{2a} = J_{2b} = J_{2c} \,. \end{aligned} \tag{2}$$

In this work we perform the fitting of the observed magnon spectrum to different models in order to find out to which extend the approximation (2) is valid for $TmFeO_3$. The anisotropy constant is practically independent of the model choice and has a value of $K_c \approx -0.09$ meV.

In a first approximation, we studied the simplest $J_1 - J_2$ model and the parameters were found to be: $J_1 = 4.92$ meV, $J_2 = 0.29$ meV, the fit quality $R_w = 2.87\%$. Note, that the results are very close to those obtained by Shapiro *et. al.* [34]. As the next step, we split the J_1 and J_2 into the in-plane component J_{ab} and perpendicular J_c. For this model we found a sensible increasing of the fit quality $R_w = 2.28\%$ and the parameters are: $J_{1ab} = 4.74$ meV, $J_{1c} = 5.15$ meV, $J_{2ab} = 0.15$ meV, $J_{2c} = 0.30$ meV and the ratios between in-plane and out of plane components J_{ab}/J_c are $\sim$0.91 for the first and $\sim$0.5 for the second coordination spheres, respectively. As a last step, we divided the in-plane parameters J_{ab} into the J_a and J_b for both coordination spheres, which gives the 6 independent exchange parameters in total. However, this approximation did not increase the fit quality significantly with the new $R_w = 2.18\%$. Furthermore, the difference between the in-plane exchange interactions was found to be below the 5% for both nearest neighbors and next-nearest neighbors, close to the standard deviation of the fitted parameters.

To summarize, our analysis indicates that a model with 4 exchange interactions provides a reliable description of the magnon excitations of the Fe subsystem in $TmFeO_3$. An excellent agreement between the calculated and observed spectra can be clearly seen in Fig. 2, which shows the constant energy cuts at $(H3L)$ and $(HK3)$ scattering planes. The exchange interactions exhibit a pronounced anisotropy with $J_c > J_{ab}$ for both coordination spheres.

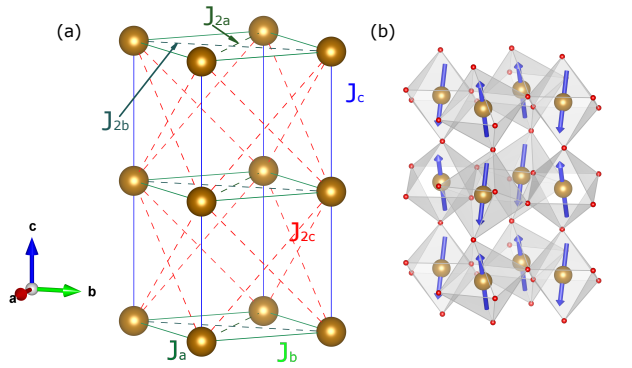

FIG. 3. (a) The sketch of the crystal structure of $TmFeO_3$ showing only positions of the Fe ions. Exchange interactions J_a, J_b, J_c, J_{2a}, J_{2b}, J_{2a} are shown by lines. (b) The sketch of the magnetic structure of $TmFeO_3$. The canting of Fe moments from the c axis is enlarged for better viewing.

B. Low-energy excitations

1. *Point-charge model calculations*

The Tm^{3+} ions in $TmFeO_3$ occupy position with C_s point group symmetry and the quantitative evaluation of the crystal field Hamiltonian requires 15 B_l^m parameters. Here we make use of a simple point-charge (PC) in order to calculate the parameters of CEF Hamiltonian [37],

$$\mathcal{H}_{\rm CEF} = \sum_{l,m} B_l^m O_l^m \ . \qquad (3)$$

We considered neighbor ions lying within a sphere of $r = 5$ Å, and used McPhase software to calculate the B_l^m parameters (the set of calculated B_l^m parameters is given in the Appendix, Table I). Using the set of parameters we modeled CEF splitting, transition intensities and magnetic anisotropy.

To check whether our parameters provide a reasonable description of the Tm^{3+} single-ion state we calculated the bulk magnetization along the different directions and compared our calculations with the experiment. Figure 5 shows the magnetization measured along three main axes at $T = 4.2$ K, together with the result of calculations. The measured magnetization is strongly anisotropic, with the easy axis pointing along the [001] direction. The c axis magnetization has a Brillouin-like shape due to the quasi-paramagnetic contribution of the Tm^{3+} ions. The estimated saturation moment of $m_c \approx 5.5 - 6\ \mu_B$ agrees with a previous report [38]. The magnetization of the Tm^{3+} ions, calculated using the PC model, well reproduces the experimental curves and predicts the type of anisotropy and values of the moment along a and c-axes, with lesser agreement for the $\mathbf{B}||b$. This disagreement may reflect a contribution of the Fe sublattice due to the Tm-Fe interactions.

We move on to consider the energy spectrum of the Tm $4f^{12}$ multiplet. According to our calculations, the CEF fully lifts the degeneracy of the ground state multiplet into 13 singlets. The first two excited levels are located at $E_1 = 1.94$ meV and $E_2 = 7.71$ meV. Only the $E_0 \to E_1$ and $E_0 \to E_2$ transitions have significant INS intensity, whereas the other transitions are at least 50 times weaker (for details, see Table II in the Appendix). The calculated energy of the first excited level is in agreement with the value obtained by means of optical spectroscopy, 2.2 meV, [39, 40], while the calculated position of the second excited level, 7.71 meV, deviates substantially from the observed experimental value of 4.8 meV.

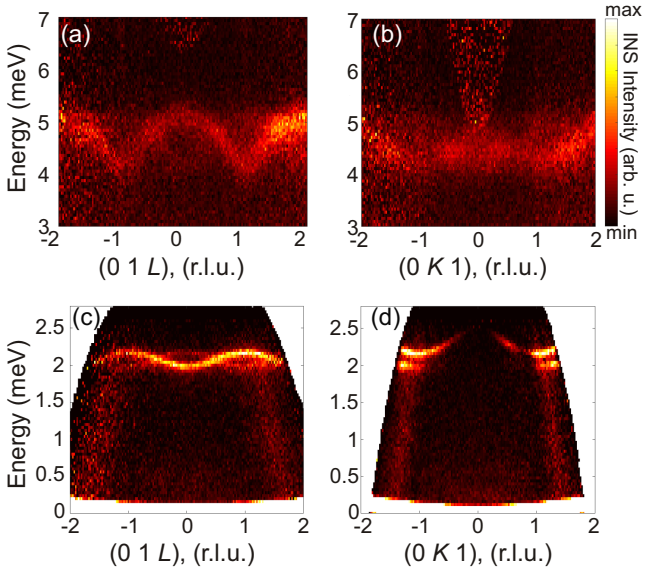

FIG. 4. Low-energy excitation spectra of $TmFeO_3$ measured in $(01L)$ (a,c) direction and $(0K1)$ (b,d) direction at $T = 1.7$ K. The spectra were taken with $E_i = 12$ meV (a,b) and $E_i = 3.3$ meV (c,d), and integrated by 0.1 r.l.u. in the orthogonal directions. The origin of the weaker but very steep vertical features is unknown.

In the energy transfer region $0 < E_f < 100$ meV, we were able to observe two low-energy excitations, at ∼2 and 5 meV, in agreement with the PC calculations. Figure 4 summarizes the important features of the excited levels. As expected, the observed excitations are dispersive due to Tm-Tm magnetic interaction. Dispersion along $(01L)$ direction is similar to the $YbFeO_3$ case for the temperatures $T < T_{SR}$ [20]. The inelastic signal consists of two modes. Their periods are shifted as $L \to L+1$. The intensity of the second mode increases with wavevector K. The second mode (sometimes called "shadow mode" [41]) has nonzero intensity for the $K \neq 0$ and appears due to the buckling of Tm atoms along the c axis, similar to the case of $YbFeO_3$ [20]. However, in contrast to the isostructural Yb-based $YbFeO_3$ and $YbAlO_3$, whose excitation has a dispersion along the L-direction only, $TmFeO_3$ exhibits dispersion with similar amplitudes along both, L and K directions.

Another remarkable result is that the dispersion bandwidth of the second excited level at ∼ 5 meV is several times larger than that of ∼ 2 meV level, probably due to

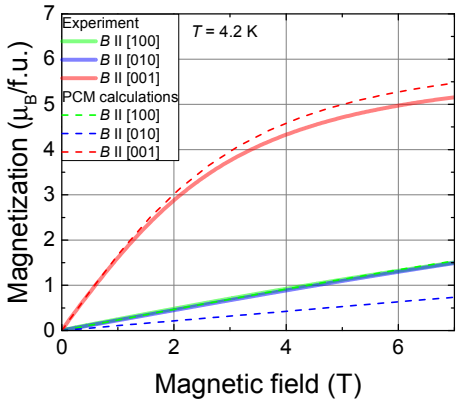

FIG. 5. Calculated and measured magnetization of $TmFeO_3$. The data are taken at $T = 4.2$ K.

higher effective moment. Moreover, the dispersion of this level is more pronounced along the L-direction, as can be seen in Fig. 4(a,b) and Fig. 6(c,d).

We now discuss the polarization of the first excited level. The low-energy excitation at 2.2 meV has no intensity for zero transferred momentum along the K and H directions. To represent this effect we made constant-energy slices within the energy of the low-lying excitation $E = [1.9, 2.3]$ meV in $(HK0)$ and $(H0L)$ planes as shown in Fig. 6(a,b). One can see a strong asymmetry of the scattered intensity for the $(H0L)$ plane, and the isotropic distribution in $(HK0)$. Such a pattern strongly resembles the polarization factor of neutron scattering for collinear magnets. However, the polarization factor has a different form for the longitudinal and transverse (including spin-wave) excitations:

$$P_{\text{Long}} = (1 - \mathbf{Q}^2) \tag{4}$$

$$P_{\text{Trans}} = (1 + \mathbf{Q}^2) \tag{5}$$

where $\mathbf{Q}$ is a unit vector parallel to the directions of the magnetic moments. Note, that the P_{Trans} factor modulates the scattered intensity by not more than a factor of 2, whereas P_{Long} completely suppresses the intensity along a direction parallel to the magnetic moment.

Figure 6(e) shows the angular dependence of the scattered intensity, integrated within the energy range $E = [1.9, 2.3]$ meV and $\mathbf{Q} \approx 1.13$ Å^{-1} in $(0KL)$ plane. We fitted the obtained curve with a simple harmonic function $I = I_0 \cdot \cos^2(\theta) + b$, and one can see that it provides a fairly good description of the data with $b \approx 0$ in agreement with the expectation for the longitudinal polarization Eq. (4). Thereby, we conclude that the 2.2 meV excitation has a longitudinal polarization, and corresponds to the moment modulation along the c axis. Note, that this conclusion is also supported by the results of our PC model calculations, which predict that the transition from the ground state to the 1.94 meV level has strongly anisotropic matrix elements with $\langle 0|J^z|1\rangle \gg \langle 0|J^x|1\rangle = \langle 0|J^y|1\rangle = 0$ (see Table II). We did not observe such a polarization for the second excited level at ~ 5 meV, which is also in a fair agreement with the PC model.

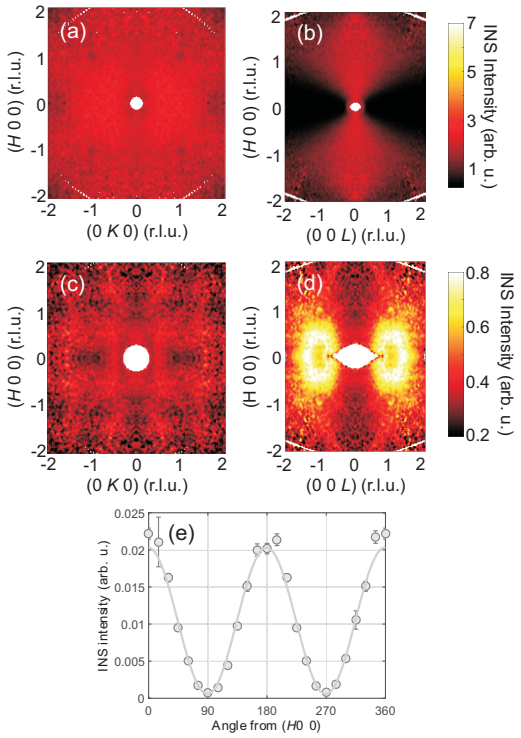

FIG. 6. Constant energy slices of the INS intensity measured at ARCS within $(HK0)$ (a, c) and $(H0L)$ (b) planes taken at $T = 7$ K. The data were integrated within the energy windows of $E = [1.9, 2.3]$ meV (a,b) and $E = [4.5, 5]$ meV. (e) Angular dependence of the INS intensity in the $(H0L)$ scattering plane. The data are integrated within the same energy window of around a constant $|\mathbf{Q}| = 1.13$ Å^{-1} with $\sim$ 0.05-0.7 (r.l.u) in orthogonal directions. The grey line shows a fit with the $\cos^2(\theta)$ function.

IV. DISCUSSIONS AND CONCLUSION

Our INS data show that the magnetic excitation spectrum of $TmFeO_3$ consists of AFM magnons within the Fe subsystem with a considerable gap of ~ 8 meV at 7 K, and two weakly dispersive CEF transitions of the Tm subsystem, which are below the gap of the Fe magnons. We described the Fe excitations using LSWT considering different combinations of exchange interactions and found that they exhibit pronounced anisotropy between in- and out-of-plane components.

The Tm dynamics is dominated by two CEF excitations, whose energies, polarization and relative intensities are reasonably well reproduced by a single-ion PC model calculation. The lowest excitations have a pronounced dispersion along both directions of the $(0KL)$ plane. This fact is in a strong contrast to the isostructural $YbFeO_3$, where only the dispersion along $(00L)$-direction was observed in the INS spectra [20]. The second excited level is also dispersive in all directions of reciprocal space, but the dispersion is stronger along the L-direction.

Usually, describing the spin dynamics of a system with

single-ion anisotropy one can start from one of the limiting cases. (i) In case of weak anisotropy ($J \gg K$) one can use a linear spin-wave theory, as we have done for the description of the magnons within the Fe subsystem. (ii) In the strong anisotropy limit, when the CEF splitting is much larger than the exchange interactions and the system has a doublet ground state, we can map the J multiplet onto the pseudo-$S = 1/2$ problem, while the single-ion anisotropy is absorbed by an effective g-tensor. One of the standard approaches (LSWT, DMRG, exact diagonalization, etc.) can be used to describe the low-energy dynamics of the doublet ground state [13, 14] in that case.

Our results show that in the case of $TmFeO_3$ the situation is more complex, because the non-Kramers ion Tm^{3+} has a magnetic singlet state, where the CEF splitting and exchange are of the same order of magnitude. Furthermore, the Tm and Fe magnetic sublattices interact, while the microscopic Hamiltonian is extremely complicated due to the low site symmetries of both Fe and Tm ions [42]. Therefore, to construct a better microscopic model for the spin dynamics, one has to separate Tm-Tm and Tm-Fe contributions, by measuring the magnetic dispersion in an isostructural material with the same CEF, but nonmagnetic transition metal ions (e.g. $TmAlO_3$). Then, one may have to perform a more sophisticated modeling of the spin dynamics taking into account both CEF and exchange, which are of the same order of magnitude. Such a complex theory is well beyond the scope of this experimental report and further theoretical work is needed to fully resolve the microscopic spin Hamiltonian of $TmFeO_3$.

ACKNOWLEDGMENTS

We thank A. Sukhanov for stimulating discussions and D. Abernathy for support with data acquisition. This research used resources at the High Flux Isotope Reactor and Spallation Neutron Source, a DOE Office of Science User Facility operated by Oak Ridge National Laboratory. S.E.N. acknowledges support from the International Max Planck Research School for Chemistry and Physics of Quantum Materials (IMPRS-CPQM). Laue x-ray diffraction measurements were conducted at the Center for Nanophase Materials Sciences (CNMS) (CNMS2019-R18) at Oak Ridge National Laboratory (ORNL), which is a DOE Office of Science User Facility.

TABLE I. Set of B_l^m (meV) parameters calculated from the PC model.

B_l^m			B_l^m		
B_2^0	=	-5.29×10^{-1}	B_6^0	=	0.2×10^{-5}
B_2^2	=	-1.35×10^{-1}	B_6^2	=	-1.1×10^{-5}
B_2^{-2}	=	12.79×10^{-1}	B_6^{-2}	=	-0.9×10^{-5}
B_4^0	=	-0.13×10^{-3}	B_6^4	=	6.1×10^{-5}
B_4^2	=	-1.7×10^{-3}	B_6^{-4}	=	0.3×10^{-5}
B_4^{-2}	=	3.29×10^{-3}	B_6^6	=	-0.9×10^{-5}
B_4^4	=	-1.22×10^{-3}	B_6^{-6}	=	-0.0×10^{-5}
B_4^{-4}	=	-9.57×10^{-3}			

TABLE II.The energy levels and out of ground state transition probabilities.

	E (meV)	$<n\|\mathrm{J}_x\|m>^2$	$<n\|\mathrm{J}_y\|m>^2$	$<n\|\mathrm{J}_z\|m>^2$
$\|E_0\rangle \rightarrow \|E_1\rangle$	1.94	0	0	27.66
$\|E_0\rangle \rightarrow \|E_2\rangle$	7.71	5.75	7.79	0
$\|E_0\rangle \rightarrow \|E_3\rangle$	14.12	0.25	0.07	0
$\|E_0\rangle \rightarrow \|E_4\rangle$	21.19	0	0	0.06
$\|E_0\rangle \rightarrow \|E_5\rangle$	33.66	0	0	0.15
$\|E_0\rangle \rightarrow \|E_6\rangle$	35.12	0.11	0.14	0
$\|E_0\rangle \rightarrow \|E_7\rangle$	50.68	0	0	0
$\|E_0\rangle \rightarrow \|E_8\rangle$	50.86	0	0	0.01
$\|E_0\rangle \rightarrow \|E_9\rangle$	72.13	0	0	0
$\|E_0\rangle \rightarrow \|E_{10}\rangle$	72.17	0	0	0.01
$\|E_0\rangle \rightarrow \|E_{11}\rangle$	105.51	0	0.01	0
$\|E_0\rangle \rightarrow \|E_{12}\rangle$	105.52	0	0	0

Appendix: Point-charge model calculations

Wavefunctions for the ground state and two low-lying levels:

$$|E\rangle_0 = -(0.024 - 0.579i)|-6\rangle + (0.318 - 0.058i)|-4\rangle + \\ +(-0.013 + 0.213i)|-2\rangle - (0.135 + 0.103i)|0\rangle + \\ +(0.202 - 0.069i)|2\rangle + (0.029 + 0.322i)|4\rangle + \\ +(-0.565 + 0.130i)|6\rangle$$

$$|E\rangle_1 = (-0.414 - 0.482i)|-6\rangle + (0.182 - 0.221i)|-4\rangle + \\ +(0.078 + 0.089i)|-2\rangle + 0.018i|0\rangle + \\ +(-0.072 + 0.094i)|2\rangle - (0.196 + 0.209i)|4\rangle + \\ +(0.382 - 0.508i)|6\rangle$$

$$|E\rangle_2 = (0.064 - 0.481i)|-5\rangle + (0.398 + 0.051i)|-3\rangle + \\ +(-0.158 + 0.281i)|-1\rangle - (0.137 + 0.292i)|1\rangle + \\ +(0.400 - 0.023i)|3\rangle + (0.029 + 0.484i)|5\rangle$$

[1] S. Sachdev, *Quantum Phase Transitions* (Cambridge University Press, 2011).

[2] L. Savary and L. Balents, "Quantum spin liquids: a review," Rep. Prog. Phys. **80**, 016502 (2016).

[3] L. D. Faddeev and L. A. Takhtadzhyan, "Spectrum and scattering of excitations in the one-dimensional isotropic Heisenberg model," J. Math. Sci. **24**, 241–267 (1984).

[4] Zh. Hao and O. Tchernyshyov, "Fermionic Spin Excitations in Two- and Three-Dimensional Antiferromagnets," Phys. Rev. Lett. **103**, 187203 (2009).

[5] B. Lake, A. M. Tsvelik, S. Notbohm, A. D. Tennant, T. G. Perring, M. Reehuis, C. Sekar, G. Krabbes, and B. Büchner, "Confinement of fractional quantum number particles in a condensed-matter system," Nature Phys. **6**, 50 (2009).

[6] B. Lake, D. A. Tennant, C. D. Frost, and S. E. Nagler, "Quantum criticality and universal scaling of a quantum antiferromagnet," Nature Materials **4**, 329–334 (2005).

[7] I. Affleck, "Bose condensation in quasi-one-dimensional antiferromagnets in strong fields," Phys. Rev. B **43**, 3215–3222 (1991).

[8] T. Giamarchi and A. M. Tsvelik, "Coupled ladders in a magnetic field," Phys. Rev. B **59**, 11398–11407 (1999).

[9] T. Fischer, S. Duffe, and G. S. Uhrig, "Microscopic model for bose-einstein condensation and quasiparticle decay," Europhysics Letters **96**, 47001 (2011).

[10] M. Mourigal, M. Enderle, A. Klöpperpieper, J.-S. Caux, A. Stunault, and H. M. Rønnow, "Fractional spinon excitations in the quantum Heisenberg antiferromagnetic chain," Nature Phys. **9**, 435 (2013).

[11] A. K. Bera, B. Lake, F. H. L. Essler, L. Vanderstraeten, C. Hubig, U. Schollwöck, A. T. M. N. Islam, A. Schneidewind, and D. L. Quintero-Castro, "Spinon confinement in a quasi-one-dimensional anisotropic heisenberg magnet," Phys. Rev. B **96**, 054423 (2017).

[12] A. Vasiliev, O. Volkova, E. Zvereva, and M. Markina, " Milestones of low-D quantum magnetism," npj Quantum Materials **3**, 18 (2018).

[13] L.S. Wu, S.E. Nikitin, Z. Wang, W. Zhu, C.D. Batista, A.M. Tsvelik, A.M. Samarakoon, D.A. Tennant, M. Brando, L. Vasylechko, M. Frontzek, A.T. Savici, G. Sala, G. Ehlers, A.D. Christianson, M.D. Lumsden, and A. Podlesnyak, "Tomonaga-Luttinger liquid behavior and spinon confinement in $YbAlO_3$," Nat. Commun. **10**, 698 (2019).

[14] L. S. Wu, W. J. Gannon, I. A. Zaliznyak, A. M. Tsvelik, M. Brockmann, J.-S. Caux, M. S. Kim, Y. Qiu, J. R. D. Copley, G. Ehlers, A. Podlesnyak, and M. C. Aronson, "Orbital-exchange and fractional quantum number excitations in an f-electron metal, Yb_2Pt_2Pb," Science **352**, 1206 (2016).

[15] W. J. Gannon, I. A. Zaliznyak, L. S. Wu, A. E. Feiguin, A. M. Tsvelik, F. Demmel, Y. Qiu, J. R. D. Copley, M. S. Kim, and M. C. Aronson, "Spinon confinement and a sharp longitudinal mode in Yb_2Pt_2Pb in magnetic fields," Nat. Commun. **10**, 1123 (2019).

[16] Y. Li, G. Chen, W. Tong, Li Pi, J. Liu, Z. Yang, X. Wang, and Q. Zhang, "Rare-Earth Triangular Lattice Spin Liquid: A Single-Crystal Study of $YbMgGaO_4$," Phys. Rev. Lett. **115**, 167203 (2015).

[17] J. A. M. Paddison, M. Daum, Zh. Dun, G. Ehlers, Y. Liu, M. B. Stone, H. Zhou, and M. Mourigal, "Continuous excitations of the triangular-lattice quantum spin liquid $YbMgGaO_4$," Nature Phys. **13**, 117 (2016).

[18] G. Hester, H. S. Nair, T. Reeder, D. R. Yahne, T. N. DeLazzer, L. Berges, D. Ziat, J. R. Neilson, A. A. Aczel, G. Sala, J. A. Quilliam, and K. A. Ross, "Novel Strongly Spin-Orbit Coupled Quantum Dimer Magnet: $Yb_2Si_2O_7$," Phys. Rev. Lett. **123**, 027201 (2019).

[19] L.-J. Chang, S. Onoda, Y. Su, Y.-J. Kao, Ku-D. Tsuei, Y. Yasui, K. Kakurai, and M. R. Lees, "Higgs transition from a magnetic Coulomb liquid to a ferromagnet in $Yb_2Ti_2O_7$," Nat. Commun. **3**, 992 (2012).

[20] S. E. Nikitin, L. S. Wu, A. S. Sefat, K. A. Shaykhutdinov, Z. Lu, S. Meng, E. V. Pomjakushina, K. Conder, G. Ehlers, M. D. Lumsden, A. I. Kolesnikov, S. Barilo, S. A. Guretskii, D. S. Inosov, and A. Podlesnyak, "Decoupled spin dynamics in the rare-earth orthoferrite $YbFeO_3$: Evolution of magnetic excitations through the spin-reorientation transition," Phys. Rev. B **98**, 064424 (2018).

[21] L. S. Wu, S. E. Nikitin, M. Brando, L. Vasylechko, G. Ehlers, M. Frontzek, A. T. Savici, G. Sala, A. D. Christianson, M. D. Lumsden, and A. Podlesnyak, "Antiferromagnetic ordering and dipolar interactions of $YbAlO_3$," Phys. Rev. B **99**, 195117 (2019).

[22] J.A. Leake, G. Shirane, and J.P. Remeika, "The magnetic structure of thulium orthoferrite, $TmFeO_3$," Solid State Commun. **6**, 15 – 17 (1968).

[23] L. T. Tsymbal, V. I. Kamenev, D. A. Khara, Ya. B. Bazaliy, and P. E. Wigen, "Structural properties of $TmFeO_3$ in the spontaneous reorientation region," Low Temperature Physics **32**, 779–782 (2006).

[24] V.P. Plakhty, Yu.P. Chernenkov, and M.N. Bedrizova, "Neutron diffraction study of weak antiferromagnetism in ytterbium orthoferrite," Solid State Commun. **47**, 309 – 312 (1983).

[25] S. Hahn, A. Podlesnyak, G. Ehlers, G. Granroth, R. Fishman, A. Kolesnikov, E. Pomjakushina, and K. Conder, "Inelastic neutron scattering studies of $YFeO_3$," Phys. Rev. B **89**, 014420 (2014).

[26] D. L. Abernathy, M. B. Stone, M. J. Loguillo, M. S. Lucas, O. Delaire, X. Tang, J. Y. Y. Lin, and B. Fultz, "Design and operation of the wide angular-range chopper spectrometer ARCS at the Spallation Neutron Source," Rev. Sci. Instrum. **83**, 015114 (2012).

[27] G. Ehlers, A. Podlesnyak, J. L. Niedziela, E. B. Iverson, and P. E. Sokol, "The new cold neutron chopper spectrometer at the spallation neutron source: design and performance," Rev. Sci. Instrum. **82**, 085108 (2011).

[28] G. Ehlers, A. Podlesnyak, and A. I. Kolesnikov, "The cold neutron chopper spectrometer at the Spallation Neutron Source - A review of the first 8 years of operation," Rev. Sci. Instrum. **87**, 093902 (2016).

[29] R. Azuah, L. Kneller, Y. Qiu, P. Tregenna-Piggott, C. Brown, J. Copley, and R. Dimeo, "DAVE: a comprehensive software suite for the reduction, visualization, and analysis of low energy neutron spectroscopic data," J. Res. Natl. Inst. Stan. Technol. **114**, 341 (2009).

[30] R. A. Ewings, A. Buts, M. D. Le, J. van Duijn, I. Bustinduy, and T. G. Perring, "HORACE: software for the anal-

ysis of data from single crystal spectroscopy experiments at time-of-flight neutron instruments," Nucl. Instrum. Methods Phys. Res. Sect. A **834**, 3132–142 (2016).

[31] O. Arnold, J. C. Bilheux, J. M. Borreguero, A. Buts, S. I. Campbell, L. Chapon, M. Doucet, N. Draper, R. Ferraz Leal, M. A. Gigg, V. E. Lynch, A. Markvardsen, D. J. Mikkelson, R. L. Mikkelson, R. Miller, K. Palmen, P. Parker, G. Passos, T. G. Perring, P. F. Peterson, S. Ren, M. A. Reuter, A. T. Savici, J. W. Taylor, R. J. Taylor, R. Tolchenov, W. Zhou, and J. Zikovsky, "Mantid – Data analysis and visualization package for neutron scattering and μSR experiments," Nucl. Instrum. Methods Phys. Res. Sect. A **764**, 156 (2014).

[32] S. Toth and B. Lake, "Linear spin wave theory for single-Q incommensurate magnetic structures," J. Phys.: Condens. Matter **27**, 166002 (2015).

[33] http://www.mcphase.de; M. Rotter, J. Magn. Magn. Mater. **272-276**, E481 (2004).

[34] S. M. Shapiro, J. D. Axe, and J. P. Remeika, "Neutron-scattering studies of spin waves in rare-earth orthoferrites," Phys. Rev. B **10**, 2014 (1974).

[35] The low-energy dataset with $E_\mathrm{i} = 25$ meV was used to determine the positions of the magnon mode at $E <$ 18 meV, and the $E_\mathrm{i} = 100$ meV spectra were used otherwise.

[36] To stabilize the correct ground state with a small spin canting [43] we have to introduce two Dzyaloshinskii-Moriya interaction constants to Eq. 1 [25]. However, both are small and have a negligible effect of the spectra.

[37] M. T. Hutchings, "Point-charge calculations of energy levels of magnetic ions in crystalline electric fields, in: Solid state physics: Advances in research and applications," (Academic Press, N.Y., 1964) pp. 227–273.

[38] Y.-J. Ke, X.-Q. Zhang, Y. Ma, and Z.-H. Cheng, "Anisotropic magnetic entropy change in $RFeO_3$ single crystals (R = Tb, Tm, or Y)," Sci. Rep. **6**, 19775 (2016).

[39] A. P. Malozemoff and R. L. White, "Optical spectra of even-electron rare earth ions in the orthoferrites," Solid State Commun. **8**, 665–668 (1970).

[40] A. P. Malozemoff, "The optical spectrum and magnetic properties of $TmFeO_3$ in the single-ion model," J. Phys. Chem. Solids **32**, 1669–1685 (1971).

[41] I. Cabrera, J. D. Thompson, R. Coldea, D. Prabhakaran, R. I. Bewley, T. Guidi, J. A. Rodriguez-Rivera, and C. Stock, "Excitations in the quantum paramagnetic phase of the quasi-one-dimensional Ising magnet $CoNb_2O_6$ in a transverse field: Geometric frustration and quantum renormalization effects," Phys. Rev. B **90**, 014418 (2014).

[42] T. Yamaguchi, "Theory of spin reorientation in rare-earth orthochromites and orthoferrites," J. Phys. Chem. Solids **35**, 479 (1974).

[43] R. L. White, "Work on the Magnetic and Spectroscopic Properties of the Rare-Earth Orthoferrites," J. Appl. Phys. **40**, 1061 (1969).